Atmos. Chem. Phys. Discuss., doi:10.5194/acp-2016-911, 2016
Manuscript under review for journal Atmos. Chem. Phys.
Published: 25 November 2016

Atmospheric Chemistry and Physics Discussions

Detecting critical $PM_{2.5}$ emission sources and their contributions to a heavy haze episode in Beijing, China by using an adjoint model

Shixian Zhai[1], Xingqin An[2], Tianliang Zhao[1], Zhaobin Sun[3,4], Qing Hou[2], Chao Wang[2]

[1]Key Laboratory for Aerosol-Cloud-Precipitation of China Meteorological Administration, Collaborative Innovation Center on Forecast and Evaluation of Meteorological Disasters, School of Atmospheric Physics, Nanjing University of Information Science & Technology, Nanjing 210044, China

[2]State Key Laboratory of Severe Weather, Key Laboratory of Atmospheric Chemistry of CMA, Chinese Academy of Meteorological Sciences, Beijing 100081, China

[3]Institute of Urban Meteorology, China Meteorological Administration, Beijing 100089, China

[4]Environmental Meteorology Forecast Center of Beijing-Tianjin-Hebei, China Meteorological Administration, Beijing, 100089, China

Correspondence to: Xingqin An (anxq@camscma.cn) and Tianliang Zhao (tlzhao@nuist.edu.cn)

Abstract. Air pollutant sources and regional transport are important issues in air quality control. The GRAPES-CUACE (Global-Regional Assimilation and Prediction System coupled with CMA Unified Atmospheric Chemistry Environment) aerosol adjoint model was applied in detecting the emission sources of a haze episode in Beijing during Nov. 19-21, 2012. Two high $PM_{2.5}$ peaks were measured respectively at 05:00 and 23:00 Beijing Time on Nov. 21st 2012, which were set as the objective functions for the aerosol adjoint model. The sensitive emission regions of the first $PM_{2.5}$ peak were tracked to the west and south to Beijing with 2-3 day cumulative transport of air pollutants to Beijing, while the sensitive emission regions of the second peak were mainly located at the south to Beijing, where southeasterly moist air transport lead to the hygroscopic growth of particles and pollutant convergence in front of the Tai-hang Mountains in the daytime of Nov. 21st. The temporal variations of the sensitivity coefficients for the two $PM_{2.5}$ concentration peaks in Beijing revealed that the response time of Beijing haze pollution to the local emissions was about 1-2 hours and to the surrounding emissions was about 7-8 hours. The contribution of surrounding emissions accounted for 67.3% and 61.0% for the first and second $PM_{2.5}$ pollution peaks respectively. The adjoint results were compared with the forward sensitivity simulations set of the Models-3/CMAQ system. Two modeling approches were well comparable in the assessments of atmospheric pollution control schemes for critical emission regions. The adjoint methods had higher computational efficiency than the forward sensitivity simulations.

Atmos. Chem. Phys. Discuss., doi:10.5194/acp-2016-911, 2016
Manuscript under review for journal Atmos. Chem. Phys.
Published: 25 November 2016

Atmospheric Chemistry and Physics Discussions

1. Introduction

The atmospheric chemistry adjoint model is a sensitivity calculation tool with high efficiency. It is developed on the basis of an atmospheric chemistry model according to the adjoint theory. Driven by the meteorological model, the source-oriented atmospheric chemistry model input emissions and output the temporal-spatial variations of pollutants. On the contrary, the receptor-oriented adjoint model inputs the gradients of the objective function to model variables, and outputs the temporal-spatial variations of the sensitivity of the objective function to any model parameters (Errico, 1997; Carmichael et al., 2008). Therefore, in concentration-source sensitivity analysis problems, the calculation efficiency of the adjoint method is much higher than that of the traditional finite difference method, which requires repeated input perturbations and results comparisons (Wang et al., 2015). Moreover, the traditional finite difference approach changes the state of the atmosphere and inevitably incurs truncation and cancellation errors (Constantin and Barrett, 2014). Nevertheless, the adjoint model integrates under certain atmospheric condition while calculating gradients, thus can provide exact sensitivities. As a result, if we set the objective function as the pollutant concentration over a region and at a time point (or during a time period), the adjoint sensitivity approach can be implemented in detecting influential emission sources in detail.

Currently, application of the adjoint model in the atmospheric environment community mainly included: source attribution of ozone (or ozone health cost) (Nester and Panitz, 2006; Martienand Harley, 2006; Pappin and Hakami, 2013; Ashok and Barrett, 2016) and $PM_{2.5}$ (Zhang et al., 2015); inverse modeling of emissions of black carbon, methane, carbon monoxide, inorganic $PM_{2.5}$ precursors etc. (Hakami et al., 2005; Bousserez et al., 2016; Paulot et al., 2014; Yumimotoand Uno, 2006; Henze et al., 2009); and aiding optimal ozone reduction policy design using adjoint-based NO_x marginal damage information (Mesbah et al., 2013).

Beijing is an economic fast growing and densely populated metropolis, and the $PM_{2.5}$ pollution problem in recent years in Beijing has become one of the focus issues of the people in various circles (Zhang et al., 2016; Sun et al., 2014; Guo et al., 2010; Wu et al., 2015). There is an urgent need to ameliorate the air pollution problem, to reduce $PM_{2.5}$ human exposure level and to improve visibility in Beijing. Till now, some researchers have estimated the contributions of local and transported pollutants to Beijing $PM_{2.5}$ (or PM_{10}) before, during and after severe pollution episodes using the flux calculation method (An et al., 2007; Jiang et al., 2015), while some others implemented the emission sources switch-on-off approach in quantifying the contributions of emissions in surrounding areas to haze in Beijing (Gao et al., 2016). Some others evaluated the expected effects of emission sources control policy through the finite difference method (Liu et al., 2014). Also, the Lagrangian particle dispersion model FLEXPART (FLEXible PARTicle dispersion model) has been used in backward tracking the potential source regions of one pollution episode (Gao et al., 2016) or of a month-long time period (Zhai et al., 2016) in Beijing. Besides, based on the sampling data, the positive matrix factorization method (PMF) or the mass balance receptor model (CMB) were also conducted in $PM_{2.5}$ source apportionment analysis (Yu et al., 2016; Zíkováet al., 2016; Liu

Atmos. Chem. Phys. Discuss., doi:10.5194/acp-2016-911, 2016
Manuscript under review for journal Atmos. Chem. Phys.
Published: 25 November 2016

Atmospheric Chemistry and Physics Discussions

et al., 2016; Zheng et al., 2005).

Previous studies can help in understanding the emission sources impacts on Beijing $PM_{2.5}$. However, the work to track the Beijing $PM_{2.5}$ sensitive sources by an adjoint model is still novel (Zhang et al., 2015). In this study, we applied the newly developed GRAPES-CUACE aerosol adjoint model (An et al., 2016) to track the sensitive emission sources of a high $PM_{2.5}$ episode in Nov. 2012 Beijing, during which time two $PM_{2.5}$ concentration peaks occurred and were set as the objective functions. We then set the average $PM_{2.5}$ concentration on 21st Nov. as the objective function and compared the adjoint results with the Models-3/CMAQ assessments (Zhai et al., 2016). This study explores the capability of the GRAPES-CUACE aerosol adjoint model in simulating the concentration-source relationships in detail, and provides guidance on the enaction of dynamic environmental control policy.

2. Synoptic analysis of the pollution episode

In combination of the Meteorological Information Comprehensive Analysis Processing System (MICAPS) results, the sounding stratification and the dew point-pressure curves at Nanjiao Station in Beijing (Figure 1), the flow field pattern, atmosphere stability and humidity over the mid-east region of China from Nov. 19th to Nov. 22nd were analyzed. Meanwhile, forming processes of two pollution peaks at the dawn and night of Nov. 21st 2012 were also qualitatively analyzed. From Nov. 19th to Nov. 20th, Beijing was under the influence of the low pressure between two high pressures. During the daytime of Nov. 19th and Nov. 20th, southerly winds prevailed below 925hPa and 1000hPa, and the relative humidity increased from Nov. 19th to Nov. 20th. During the nighttime of Nov. 19th and Nov. 20th, southerly winds transformed to northeasterly and easterly winds, which brought pollutants together with water vapor to Beijing. Meanwhile, thermal inversion existed below 850hPa on Nov. 19th and Nov. 20th. The above analysis revealed that $PM_{2.5}$ concentration accumulation from Nov. 19th to Nov. 20th was tightly connected with the southerly wind at daytime and the easterly wind at nighttime.

During the daytime on Nov. 21st, Beijing-Tianjin-Hebei area was at the bottom of the high pressure with easterly wind prevailed on the 850hPa layer, thermal inversion maintained and relative humidity continued increasing. The mid-south Hebei was influenced by weak cold air and was controlled by northerly winds, and Beijing was mainly under the influence of the easterly wind that promoted pollutants convergence in front of the Tai-hang Mountains and carried abundant water vapor which accelerated hygroscopic growth of local particles. It can be seen that the pollution peak at the night of Nov. 21st was not only the result of pollutants accumulation during the ahead 2 days, but also the result of hygroscopic growth of local particles and pollutants convergence caused by the easterly wind at the daytime of Nov. 21st. According to previous researches (Chen et al., 2016; Li et al., 2016), this was a typical synoptic episode that gradually generate air pollutants over Beijing until a sudden and significant improvement of air quality resulted from strong winds. This was also the same episode that was analyzed in Zhai et al. (2016), thus facilitating further comparisons.

Atmos. Chem. Phys. Discuss., doi:10.5194/acp-2016-911, 2016
Manuscript under review for journal Atmos. Chem. Phys.
Published: 25 November 2016

Atmospheric Chemistry and Physics Discussions

3. Methods

3.1. Concepts of adjoint sensitivity analysis

Sensitivity analysis plays an important role in the atmospheric environment community. Knowledge of emission sources impacts on pollutant concentration can help enacting air pollution control strategies. The adjoint model is of great efficiency in calculating the sensitivity of an objective function to any model variable at any time-step. To explicitly explain the concepts of an adjoint model, Fig. 1S (in the supplement) illustrates the schematic diagrams of the atmospheric chemistry forward and adjoint models. The atmospheric chemistry model takes emissions (**S**: S_1, S_2, …, S_n, …, S_N) as inputs and outputs pollutant concentrations (**C**: C_1, C_2, …, C_m, …, C_M) through forward integration. As any emission source S_n might has an influence on the concentration at every receptor site C_m, a pair of emission sources sensitivity tests through the traditional source-oriented finite difference method can obtain the contribution from one emission source (or a combined group of emission sources) to pollutants at any receptor site. Therefore, with **N** emission sources and **M** receptors in total, the pollutant contribution from each one of the **N** emission sources to each of the **M** receptors (a **N**×**M** matrix) can be obtained through **N** times of forward integration. That is, computational load increases proportionally with the increase of **N**.

The receptor-oriented adjoint model is complementary to the forward model. The sensitivity map of a scalar function of pollutant concentration (the objective function) to every emission source (**N**×1 matrix) can be obtained through one backward adjoint integration (Sandu, 2005; An et al., 2016; Zhai, 2015). Therefore, the above-mentioned **N**×**M** matrix needs **M** times of adjoint integrations. Theoretically, the resulting **N**×**M** matrix from the forward and backward methods are the same within a small perturbation (Liu, 2005). Therefore, an atmospheric chemistry model is suitable for air pollution processes simulation and an adjoint model is efficient in quantifying receptor-source relationships (Liu, 2005).

The adjoint model can work out the sensitivity of the objective function **J** to any emission source S_n: $\partial \mathbf{J}/\partial S_n$. If we are comparing a group of uniformly distributed emission sources, the larger the $\partial J/\partial S_n$ is, the bigger its influence has on **J.** However, obvious discrepancies of emission intensities existed between urban and rural areas, together with the seasonal and diurnal changes. Besides, emissions of different species might have different units and may differ in the order of magnitudes. Under these circumstances, relative contribution of each emission source can't be determined only by the gradient $\partial J/\partial S_n$. Therefore, we define the sensitivity coefficients in this study as: $(\partial J/\partial S_n)\cdot S_n$, which shares the same unit with the objective function, and can reflect exact contribution of each emission source to the objective function, thus making comparisons among emissions more convenient.

3.2. Model description

The GRAPES-CUACE (Global-Regional Assimilation and Prediction System coupled with CMA Unified Atmospheric Chemistry Environment) is an on-line coupled atmospheric-chemistry modeling system (Wang et al., 2009; Zhou et al., 2012;

Atmos. Chem. Phys. Discuss., doi:10.5194/acp-2016-911, 2016
Manuscript under review for journal Atmos. Chem. Phys.
Published: 25 November 2016

Jiang et al., 2015) developed by the China Meteorological Administration (CMA). In GRAPES-CUACE, GRAPES-Meso is a regional meteorological model (Xue et al., 2008), and CUACE is an atmospheric chemistry modeling system independent of meteorological and climate models (Gong et al.，2009). The CUACE system is compatible with various kinds of meteorological models and can be used as a common platform for atmospheric constituent calculation.

The GRAPES-CUACE aerosol adjoint model, developed on the basis of the GRAPES-CUACE modeling system according to the adjoint theory, includes the adjoint of the size-segregated multi-component aerosol algorithm CAM (Canadian Aerosol Module, Gong et al., 2003), the adjoint of the three interface programs that connected GRAPES-Meso and CUACE, and the adjoint of the aerosol transported processes. As CAM includes major aerosol processes in the atmosphere: generation, hygroscopic growth, coagulation, nucleation, condensation, dry deposition/sedimentation, below-cloud scavenging, aerosol activation, and chemical transformation of sulfur species in clear air and in clouds (Gong et al., 2003), the GRAPES-CUACE aerosol adjoint model is capable of simulating sensitivities of the objective function to primary aerosol sources while coupling major aerosol processes described above.

Figure S2 shows the operational processes in this study. Before carrying out the adjoint simulation, the forward GRAPES-CUACE model should be integrated to save the unequilibrated variables in checkpoint files at the beginning of each external time step. Then the saved variables were input at each check point during the backward adjoint integration. As for intermediate unequilibrated variables, recalculation and stack storage (PUSH & POP) schemes were adopted. Details about the construction, framework and operation flowchart of the GRAPES-CUACE aerosol adjoint model were discussed in paper An et al. (2016).

3.3. Model setup and validation

The simulated domain in this study covered northeast China (105-125°E, 32.25-42.25°N) (Figure 2), which included 41×23 simulation grid cells at the resolution of 0.5°×0.5°. With 31 vertical layers, the model integrated at a time step of 300s. The INTEXB-2006 with 0.5°×0.5° resolution (Zhang et al., 2009) that includes five aerosol species of black carbon (BC), organic carbon (OC), sulfate, nitrate, and fugitive dust particles, in addition to 27 gases, such as VOCs, NH_3, CO, CO_2, SO_x and NO_x (An et al., 2013) was implemented as the emissions inventory. The National Centers for Environmental Prediction (NCEP) Final Analysis (FNL) data set were used as the initial meteorological field and the meteorological boundary condition. The chemical initial and boundary values were set as the observed monthly means, and the initial values of all chemical species were from the 24 h forecast made by the previous day's simulation. To eliminate the discrepancy between idealized initial concentration field and the real concentration field, simulation started from 20:00 BT (Beijing Time) Nov. 15th, and the analyzed period was from 20:00 BT Nov. 18th to 20:00 BT Nov. 22nd.

Figure 3a shows the comparisions of the observed and simulated hourly $PM_{2.5}$ concentration curves from 20:00 BT Nov. 18th 2012 to 20:00 BT Nov. 22nd 2012 and their scatter plots at the Chinese Research Academy of Environmental Sciences

Atmos. Chem. Phys. Discuss., doi:10.5194/acp-2016-911, 2016
Manuscript under review for journal Atmos. Chem. Phys.
Published: 25 November 2016

Atmospheric Chemistry and Physics Discussions

(CREAS) observation station. The CRAES station provides measured $PM_{2.5}$ concentrations locates in the northwest Chaoyang District at the Chinese Academy of Environmental Sciences and can be viewed as a representative urban observation station in Beijing (Zhai et al., 2016).

Figure 3a reveals that the results of the GRAPES-CUACE modeling system corresponded well with the synoptic analysis of the pollution episode. The modeling system reproduced the $PM_{2.5}$ accumulation processes from Nov. 19th to Nov. 21st in Beijing, and captured the two $PM_{2.5}$ hourly concentration peaks at the dawn and night of Nov. 21st as well as the trough at Nov. 21st afternoon with a correlation coefficient of 0.93, even though the model overestimated the $PM_{2.5}$ concentration values over the simulation period, which might attribute to the coarse resolution of the model settings (0.5°×0.5°) and the local environmental interference on the observation site. In addition, pre-existing studies (Zhou et. al., 2012; Wang et al., 2015a; Wang et. al., 2015b; Jiang et. al., 2015) had convinced the stable simulation performance of the GRAPES-CUACE modeling system in reproducing air pollution levels and variation trends over northeast China. Above all, the following analysis mainly focused on the variations and contribution proportions of emission sources over different regions, thus analyzing results based on this simulation was considered reliable.

3.4. Simulated haze episode

Figure 4 shows the simulated surface $PM_{2.5}$ concentration and wind field variations from 17:00 BT Nov. 19th 2012 to 11:00 BT Nov. 22nd 2012. It can be seen that the simulation results were consistent with the above weather analysis. From Nov. 19th to Nov. 20th, $PM_{2.5}$ concentration in Beijing accumulated under the influence of convergent wind field pattern: southerly wind field to the south, easterly wind field to the east, and westerly wind field to the west. Till 5:00 BT to 11:00 BT Nov. 21st, $PM_{2.5}$ concentration value exceeded 550μg/m^{3}over southern Beijing, south central Hebei as well as northwest Tianjin. Thereafter, $PM_{2.5}$ concentration over Beijing, south central Hebei and Tianjin decreased before rising above 550μg/m^3 at 23:00 BT. That was because on Nov. 21st, under the influence of the easterly winds, pollutants converged ahead of the Tai-hang Mountains, and abundant water vapor was carried into Beijing and promoted local hygroscopic growth. Afterwards, during the daytime of Nov. 22nd, notable northwesterly wind dispersed pollutants in Beijing and ended this pollution episode.

3.5. Objective function

Same as the simulated and the observed hourly $PM_{2.5}$ concentration variations at CREAS station, Beijing municipality also witnessed two hourly $PM_{2.5}$ concentration peaks at 5:00 BT and 23:00 BT Nov. 21st 2012 (Figure 3b), which directly lead to the high $PM_{2.5}$ concentration on Nov. 21st, the same pollution peak day analyzed in a previous research (Zhai et al., 2016). In order to analyze the critical emission sources of the two hourly $PM_{2.5}$ concentration peaks, we take advantage of the adjoint model in simulating concentration-emission relationships and defined two objective functions as: hourly mean $PM_{2.5}$ concentration over Beijing at ①5:00 BT and ②23:00 BT of Nov. 21st 2012. Then, in order to demonstrate the reliability

Atmos. Chem. Phys. Discuss., doi:10.5194/acp-2016-911, 2016
Manuscript under review for journal Atmos. Chem. Phys.
Published: 25 November 2016

and high-efficiency of the GRAPES-CUACE aerosol adjoint model in providing guidance on high-effective and high-efficient air quality control schemes design, a third objective function was defined as: ③average $PM_{2.5}$ concentration over Beijing on 21st Nov. Subsequently, comparisons between results from the GRAPES-CUACE aerosol adjoint model and the Models-3/CMAQ assessments (Zhai et al., 2016) were made.

4. Results

4.1. Sensitivity coefficients distribution of primary $PM_{2.5}$ emission sources

Figure 5 illustrates the time-integrated sensitivity coefficients of the two hourly Beijing $PM_{2.5}$ concentration peaks to emission sources. The sensitivity coefficients of the objective function to emission sources connected pollutants with emissions, and revealed the emissions impacts on peak $PM_{2.5}$ concentrations. The larger the sensitivity coefficient value is, the greater its influence has on the objective function *J*. For example, the largest sensitivity coefficient in Figure 5d covers Daxing district with a value of 22.4μg/m^3, which indicated that emissions emitted over this grid area had the greatest influence on the peak concentration. If emissions were reduced within a small range, decrease of $PM_{2.5}$ concentration could be viewed as linearly. For example, if *N*% emissions were reduced over this grid cell from 05:00 BT Nov. 18th 2012 to 05:00 BT Nov. 21st 2012, objective $PM_{2.5}$ concentration would decrease by *N*%*22.4μg/m^3.

In Figure 5a and d and Figure 5e and h, with the accumulation along backward time sequence, the more influential regions (regions with relatively larger sensitivity coefficients) extended from local Beijing to its surrounding provinces. This phenomenon reflected that in this pollution episode, $PM_{2.5}$ in Beijing was not only the results of local emissions, but also the results of emissions from surrounding regions including Hebei province, Tianjin city and even Shanxi and Shandong provinces. Emissions from the surrounding areas continuously transported to Beijing 2-3 days ahead of the peak polluted day, and lead to the continuous increase of Beijing air pollutants concentration.

There were differences between the variations of the more sensitive emission regions of this two $PM_{2.5}$ concentration peaks. Firstly, comparing the 12-hour time cumulated sensitivity coefficients distribution in Figure 5b and f, we can see that emissions to the southwest of Beijing already had a clearly influence on the 05:00 BT Nov. 21st $PM_{2.5}$ concentration peak (Figure 5b), however, for the 23:00 BT Nov. 21st $PM_{2.5}$ concentration peak, influential emission sources still concentrated over Beijing municipality (Figure 5f), with only a small fraction of influential emissions from east and south to Beijing. This was due to the southwest airstream to the southwest of Beijing from 23:00 BT Nov. 20th to 05:00 BT Nov. 21st and the southeasterly water vapor import on Nov. 21st afternoon to night which caused moisture absorption growth of local particles and the input of pollutants from Tianjin.

Secondly, it can be seen from the 24-h (Figure 5c and g) and 72-h (Figure 5d and h) time cumulative sensitivity coefficients distributions that sensitivity coefficients over both local and surrounding Beijing have relatively large values. This reflected

Atmos. Chem. Phys. Discuss., doi:10.5194/acp-2016-911, 2016
Manuscript under review for journal Atmos. Chem. Phys.
Published: 25 November 2016

Atmospheric Chemistry and Physics Discussions

that both of these two $PM_{2.5}$ concentration peaks were influenced by local and surrounding emissions. Take a further comparison, the more influential emission regions of the two $PM_{2.5}$ concentration peaks differed. For the first $PM_{2.5}$ concentration peak, 24-h cumulated influential source regions (Figure 5c) distributed over Beijing and the west and south to Beijing, and the 72-h cumulated influential source regions (Figure 5g) spread northeastward to Shanxi province. However, For the second $PM_{2.5}$ concentration peak, time-cumulated influential source regions mainly located at the south of Beijing, and the 72-h cumulated influential source regions over west to Beijing (Shanxi province) (Figure 5h) covered a smaller area than that for the first $PM_{2.5}$ concentration peak (Figure 5d).

The above phenomenon showed that the variation of the sensitivity coefficients distribution, the meteorological condition and the pollution evolution processes corresponded with each other very well. Meanwhile, this indicated that, the adjoint model is powerful to quantitatively reproduce the generating processes of an air pollution episode from pollutants to emissions backward in time.

4.2. Hourly variations of sensitivity coefficients and overall proportions of local and surrounding emission sources contribution to peak $PM_{2.5}$ concentrations

Figure 6 illustrates the hourly instantaneously sensitivity coefficients to local and surrounding emission sources (Figure 6a and b), their corresponding time integrated series (Figure 6c and d) and the contribution ratios of local and surrounding emission sources to the $PM_{2.5}$ concentration peaks (Fig. 6e and f). It can be seen that along with the time reversed integration, instantaneous sensitivity coefficients of the $PM_{2.5}$ concentration peaks to local (red solid square) and surrounding (red hallow square) emissions ascended to their maxima before showing a decreasing tendency. Meanwhile, detailed comparisons of the local and surrounding emissions hourly contribution revealed their significant differences.

Analyzing Figure 6a and b along reversed time sequence, the peaks of the local emission sensitivity coefficients (red solid square) and the $PM_{2.5}$ concentration peaks (blue solid circle) appeared at almost the same time, with the latter delayed for 1-2 hours. This indicated that local emissions emitted 1-2 hours ahead of the $PM_{2.5}$ peak values have the largest influence on the peak pollution. Analyzing along reversed time sequence (Figure 6a and b), we can see that for the first $PM_{2.5}$ concentration peak, local emissions emitted 19 hours ahead of the pollution peak and earlier have negligible contribution with tiny fluctuation (Figure 6a). Similarly, for the second $PM_{2.5}$ concentration peak, local emissions emitted 14 hours ahead of the $PM_{2.5}$ concentration peak and earlier only have very little influence. This revealed that $PM_{2.5}$ generated from local emissions can be transported to the downstream to Beijing after 14-19 hours.

In contrast, peak sensitivity coefficients of the surrounding emissions (red hallow square) were 7-9 hours ahead of the $PM_{2.5}$ concentration peaks (Figure 6a and b), which indicated that influence of emissions from surrounding areas to Beijing $PM_{2.5}$ concentration reached their peaks 7-9 hours ahead of the pollution peak. Then along with backward integration, sensitivity coefficients showed overall decreasing trends together with periodic fluctuations. For the first $PM_{2.5}$ concentration peak

Atmos. Chem. Phys. Discuss., doi:10.5194/acp-2016-911, 2016
Manuscript under review for journal Atmos. Chem. Phys.
Published: 25 November 2016

Atmospheric Chemistry and Physics Discussions

(05:00 BT Nov. 21st), relative maximum contribution from surrounding areas (Figure 6a) appeared at 20:00 BT Nov. 20th, 2:00 BT Nov. 20th and 5:00 BT Nov. 19th respectively along time-reversed sequence. The first time-reversed relative maximum sensitivity coefficient at 20:00 BT Nov. 20th was 7.2μg/m^3, far greater than the local sensitivity coefficients (3.3μg/m^3) at the same moment, while the second time-reversed relative maximum sensitivity coefficient at 2:00 BT Nov. 20th was 4.7μg/m^3, remarkably decreased from the first one. For the second $PM_{2.5}$ concentration peak (23:00 BT Nov. 21st) (Figure 6b), relative maximum contribution from surrounding areas (red hallow square) appeared at 16:00 BT Nov. 21st, 20:00 BT Nov. 20th, 2:00 BT Nov. 20th and 3:00 BT Nov 19th. The first time-reversed relative maximum sensitivity coefficient (5.1μg/m^3) of the surrounding emissions was smaller than the local sensitivity coefficient (7.1μg/m^3) at the same moment. The second time-reversed relative maximum sensitivity coefficient (5.0μg/m^3) was about the same as the first one. This was because the second $PM_{2.5}$ concentration peak was cumulated on the base of the first high $PM_{2.5}$ concentration peak, thus emissions from the surrounding areas at 20:00 BT Nov. 20th also had a large influence on the second $PM_{2.5}$ concentration peak, and even almost equal to the first relative maximum contribution at 16:00 BT Nov. 21st.

Besides, analyzing the time-cumulated sensitivity coefficients series (Figure 6c and d) along reversed time sequence, we can see that for both $PM_{2.5}$ concentration peaks, the dominate emission source areas transformed from the local to the surroundings. For the first $PM_{2.5}$ concentration peak (05:00 BT Nov. 21st) (Figure 6c), the time-cumulated local emission sensitivity coefficients (red solid square) were larger than the time-cumulated surrounding emission sensitivity coefficients (red hallow square) from 11:00 BT Nov. 20th to 05:00 BT Nov. 21st(11 hours), which indicates that local emissions dominated during this 11-hour time period. Yet for the second $PM_{2.5}$ concentration peak (23:00 BT Nov. 21st) (Figure 6d), local emissions influence dominated from 17:00 BT Nov. 20th to 23:00 BT Nov. 21st, which lasted for 31 hours, threefold of that of the first $PM_{2.5}$ peak pollution. This phenomenon again indicated the tiny effect of emissions transportation processes on Nov. 21st, and the increase of $PM_{2.5}$ concentration on Nov. 21st was mainly due to local generation. The above phenomena reflected that local emissions impacts on the second $PM_{2.5}$ concentration peak were larger than that on the first $PM_{2.5}$ peak. In another way, it revealed that impacts of surrounding emissions on the first $PM_{2.5}$ concentration peak were rather impressive.

Analyzing the hourly sensitivity coefficients along reversed time sequence in Figure 6a and b, it can be seen that the hourly contribution of both the local (red solid square) and surrounding (red hallow square) emissions had negligible impacts on the $PM_{2.5}$ concentration peaks three days (72 hours) ahead of the objective time points. Therefore, comparing the time-cumulated sensitivity coefficients at 72 hours ahead of the two $PM_{2.5}$ concentration peaks, we can obtain the local and surrounding emissions contribution percentages to these two $PM_{2.5}$ concentration peaks (Figure 6e and f). Surrounding emissions had larger impacts on both of the two $PM_{2.5}$ concentration peaks than local emissions, and the impacts of surrounding emissions on the first $PM_{2.5}$ concentration peak was greater than that on the second $PM_{2.5}$ concentration peak. For the first $PM_{2.5}$ concentration peak (at 05:00 BT Nov. 21st), surrounding emissions accounted for 67.3% while it was 32.7% for local

Atmos. Chem. Phys. Discuss., doi:10.5194/acp-2016-911, 2016
Manuscript under review for journal Atmos. Chem. Phys.
Published: 25 November 2016

Atmospheric Chemistry and Physics Discussions

emissions (Figure 6e); for the second $PM_{2.5}$ concentration peak (at 23:00 BT Nov. 21st), surrounding emissions contributed 61.0% while local emissions contributed 39.0% (Figure 6f). It can be inferred from the local and surrounding emissions hourly sensitivity coefficients time series that due to the general circulation of the atmosphere and the local circulation at Beijing, contribution from the surrounding emissions to the peak $PM_{2.5}$ had an obvious periodic fluctuation, thus leading to the notable contribution from surrounding emissions to peak $PM_{2.5}$ concentration. Therefore, if joint control of pollutant emissions with Hebei province, Tianjin city and Shanxi province were implemented 2-3 days ahead of the first $PM_{2.5}$ concentration peak, then $PM_{2.5}$ concentration accumulation due to transported pollutants could be effectively prevented, thus decreasing the concentration of these two $PM_{2.5}$ concentration peaks.

4.3. Comparisons of the adjoint results with Models-3/CMAQ assessments

Based on a previous research in which the back-trajectory model FLEXPART was used in locating sensitive emission regions of the Beijing $PM_{2.5}$ concentration in Nov. 2012, and the Models-3/CMAQ modeling system was then used in quantifying the effects of emission reduction schemes (at different ratios, during different times and over different regions) in reducing $PM_{2.5}$ concentration on Nov. 21st in Beijing (Zhai et al., 2016), we then set the average $PM_{2.5}$ concentration on 21st Nov. as the objective function and compared the adjoint results with the Models-3/CMAQ assessments.

Figure 7 illustrates the time integrated sensitivity coefficient distributions when the Beijing average $PM_{2.5}$ concentration on Nov. 21st was set as the objective function. Corresponded with previous research that advocated cooperation with surrounding provinces 2-3 days ahead of the most polluted day, adjoint time integrated sensitivity coefficients extended and intensified along 48-72h backward time integration. In order to assess source contribution from different regions, we refer to the research by Zhai et al. (2016) and defined four emission regions according to the adjoint results: the overall Huabei region (HuaB), the sensitive Huabei region (HuaB-sens), the overall Beijing municipality (BJ), and the sensitive Beijing region (BJ-sens) (Figure 8). In this research, grid cells with 72-h sensitivity coefficient larger than $3\mu g/m^3$ were chosen as the sensitive emission regions. The threshold value was chosen based on the relative magnitude of the sensitivity coefficients and the corresponding sources contribution ratios of sensitive regions to the objective function. Here the HuaB-sens accounts for 10.2% the area of HuaB and the BJ-sens accounts for 60.0% the area of BJ (Figure 8).

From the emission sources contribution ratios to the peak $PM_{2.5}$ concentration (Table 1) and the contrast of sensitive and full regions emission sources contributions to the peak $PM_{2.5}$ concentration (Table 2), we can see that the adjoint results consisted very well with all conclusions from the assessments of critical source regions emission reduction schemes quantified by the Models-3/CMAQ system (Zhai et al., 2016).

Firstly, the Nov. 21st $PM_{2.5}$ concentration was an accumulated result from emissions 1-2 days ahead of the most polluted day till that day, rather than just an instinct result of emissions on Nov. 21st. For all four regions, emissions contribution ratios grew from 'd0' to 'd2' (implications of 'd0', 'd1' and 'd2' are listed below Table 1), especially from 'd0' to 'd1'. The contribution

Atmos. Chem. Phys. Discuss., doi:10.5194/acp-2016-911, 2016
Manuscript under review for journal Atmos. Chem. Phys.
Published: 25 November 2016

Atmospheric Chemistry and Physics Discussions

ratios of emissions from BJ (or BJ-sens) and HuaB (or HuaB-sens) from 'd0' to 'd1' increased 6.2% (or 5.7%) and 32.0% (or 18.9%). Thereafter, the sources contribution ratios again increased by 0.6% (or 0.5%) and 9.6% (or 3.6%) for emissions over BJ (or BJ-sens) and HuaB (or HuaB-sens) from 'd1' to 'd2'.

Secondly, the above phenomenon also indicated that, with the accumulation of backward integration from 48h to 72h prior to Nov. 21st, emission sources contribution from HuaB (or HuaB-sens) to peak $PM_{2.5}$ concentration increased obviously, while emission sources contribution from BJ (or BJ-sens) hardly increased. This can be explained by the role of pollutant transmission that surrounding emissions can continuously transport to Beijing 2-3 days ahead of the most polluted day (Zhai et al., 2016).

Thirdly, the contribution efficiency (contribution ratios per grid cell) of emissions from the HuaB-sens and BJ-sens were significantly higher than that from the corresponding entire HuaB and BJ regions respectively. Although BJ-sens accounted only 60% the area of the entire BJ, its contribution to the peak $PM_{2.5}$ concentration was 86.6%-88.2% of that of the entire BJ and its source contribution efficiency was 1.4 to 1.5 times that of BJ. Similarly, HuaB-sens accounted only 10.2% the area of the entire HuaB, its contribution to the peak $PM_{2.5}$ concentration was 71.9% of that of the entire HuaB and its source contribution efficiency was 6.0-7.0 times that of the entire HuaB (Table 2). Last but not least, emissions from HuaB-sens contributed much more than emissions only from BJ-sens, which supported joint control.

5. Conclusions

In this research, the GRAPES-CUACE aerosol adjoint model was applied to detect the pivotal emission sources of a Nov. 2012 haze episode, and the hourly peak $PM_{2.5}$ concentrations at 05:00 BT and 23:00 BT Nov. 21st 2012 over Beijing were set as the objective functions. On this basis, contributions to peak $PM_{2.5}$ concentration peaks from local and surrounding Beijing were compared. It turned out that the adjoint results corresponded very well with the real weather analysis, and could reasonably reflect that the more influential emission sources for the first $PM_{2.5}$ concentration peak mainly spread over local Beijing and the west and south to Beijing in Hebei and Shanxi provinces due to transmission of pollutants 2-3 days ahead of the peak time. However, the more sensitive emission sources for the second $PM_{2.5}$ concentration peak mainly concentrated over local Beijing and the south to Beijing in Hebei province for the reason that the second $PM_{2.5}$ concentration peak was accumulated on the basis of the first $PM_{2.5}$ concentration peak due to local particles hygroscopic growth and pollutants convergence ahead of the Tai-hang Mountains on Nov. 21st. Beijing $PM_{2.5}$ concentration peak responded to local emissions in 1-2 hours while to surrounding emissions in 7-8 hours. Surrounding emissions contribution proportion for the first $PM_{2.5}$ concentration peak was 67.3%, larger than that for the second $PM_{2.5}$ concentration peak, which was 61.0%.

We then set the average Beijing $PM_{2.5}$ concentration on Nov. 21st as another objective function and compared adjoint results with Models-3/CMAQ assessments. It was shown that the adjoint results can provide all the conclusions made by the

Models-3/CMAQ assessments (Zhai et al., 2016). Joint controlling measures focused on sensitive emission regions (regions detected by an adjoint model or the FLEXPART model) implemented 2-3 days ahead of the predicted pollution peak day can help reduce emissions control costs as well as improve the controlling efficiency and maneuverability. Beyond that, the computational loads of the adjoint simulation were much smaller than the work in Models-3/CMAQ assessments (Zhai et al., 2016). For the adjoint simulation, one forward integration (for un-equilibrated data saving) and one adjoint backward integration could obtain the influence of emissions from any emission region, during any time period to the peak $PM_{2.5}$ concentration. However, in the Models-3/CMAQ assessments, in order to compare the effects of emission reduction strategies over two different time periods, at two different ratios and over four different regions, 12 sensitivity tests were set and the forward model was integrated for 13 times (one basic simulation included).

In conclusion, this research showed that the adjoint method is very powerful in simulating the concentration-emission relationship backward in time and can be utilized in helping make dynamic air quality control schemes.

Acknowledgement

This work was supported by the National Nature Science Foundation of China (41575151), the National Science-technology Support Plan Projects (2014BAC16B03), the Beijing Municipal Science & Technology Commission (Z131100006113013) and the Program for Postgraduate Research Innovation of Jiangsu Higher Education Institutions (KYZZ16_0346).

References

An, X. Q., Sun, Z. B., Lin, W. L., Jin, M., and Li, N.: Emission inventory evaluation using observations of regional atmospheric background stations of China, J. Environ. Sci., 25, 537-546, 2013.

An, X. Q., Zhai, S. X., Jin, M., Gong, S. L., and Wang, Y.: Development of an adjoint model of GRAPES–CUACE and its application in tracking influential haze source areas in north China, Geosci. Model Dev., 9, 2153-2165, 2016.

An, X. Q., Zhu, T., Wang, Z. F., Li, C. Y., and Wang, Y. S.: A modeling analysis of a heavy air pollution episode occurred in Beijing, Atmos. Chem. Phys., 7(12), 3103-3114, 2007.

Ashok, A. and Barrett, S.: Adjoint-based computation of U.S. nationwide ozone exposure isopleths, Atmos. Environ., 133: 68-80, 2016.

Bousserez, N., Henze, D. K., Rooney, B., Perkins, A., Wecht, K. J., Turner, A. J., Natraj, V., and Worden, J.: Constraints on methane emissions in North America from future geostationary remote sensing measurements, Atmos. Chem. Phys., 16, 6175-6190, 2016.

Carmichael, G. R., Sandu, A., Chai, T. F., Daescu, N. D., Constantinescu, E. M., and Tang Y. H.: Predicting air quality: Improvements through advanced methods to integrate models and measurements, Journal of Computational Physics., 227(7):

3540-3571, 2008.

Constantin, B. V. and Barrett, S. R.: Application of the complex step method to chemistry-transport modeling, Atmos. Environ., 99: 457-465, 2014.

Chen, Z. Y., Xu, B., Cai, J., and Gao B. B.: Understanding temporal patterns and characteristics of air quality in Beijing: A local and regional perspective, Atmos. Environ., 127: 303-315, 2016.

Errico, R. M.: What is an adjoint model? Bulletin of the American Meteorological Society, 78(11), 2577-2591, 1997.

Gao, M., Carmichael, G. R., Wang, Y., Saide, P. E., Yu, M., Xin, J., Liu, Z., and Wang, Z.: Modeling study of the 2010 regional haze event in the North China Plain, Atmos. Chem. Phys., 16(3), 1673-1691, 2016.

Guo, Y. M., Tong, S. L., Li, S. S., Barnett, A. G., Yu, W. W., Zhang, Y. S., and Pan, X. C.: Gaseous air pollution and emergency hospital visits for hypertension in Beijing, China: a time-stratified case-crossover study, Environmental Health, 9(1), 57, 2010.

Hakami, A., Henze, D. K., and Seinfeld, J. H.: Adjoint inverse modelling of black carbon during the Asian Pacific Regional Aerosol Characterization Experiment, Journal of Geophysical Research, Vol. 110, D14301, 2005.

Henze, D. K., Seinfeld, J. H., and Shindell, D. T.: Inverse modeling and mapping US air quality influences of inorganic PM 2.5 precursor emissions using the adjoint of GEOS-Chem, Atmos. Chem. and Phys., 9(16) ,5877-5903, 2009.

Jiang, C., Wang H., Zhao T. L., Li T., and Che H.: Modeling study of $PM_{2.5}$ pollutant transport across cities in China's Jing-Jin-Ji region during a severe haze episode in December 2013, Atmos. Chem. Phys., 15(10), 5803-5814, 2015.

Li, L. J., Wang, Z. S., Zhang, D. W., Chen, T., Jiang, L., and Li, Y. T.: Analysis of heavy air pollution episodes in Beijing during 2013-2014, China Environmental Science, 36(1): 27-35, 2016 (in Chinese).

Liu, F.: Adjoint model of Comprehensive Air quality Model CAMx – construction and application, Peking University Post-doctoral Reseach Report, 2005 (*in Chinese*).

Liu, J., An, X. Q., Zhu, T., Zhai, S. X., and Li, N.: Evaluation of $PM_{2.5}$ decrease in Beijing after emission restrictions in the Beijing-Tianjin-Hebei and surrounding, China Environ. Sci. 34 (11), 2726-2733, 2014 (in Chinese).

Liu, Q. Y., Baumgartner, J., Zhang, Y. X., and Schauer, J. J.: Source apportionment of Beijing air pollution during a severe winter haze event and associated pro-inflammatory responses in lung epithelial cells, Atmos. Environ., 126, 28-35, 2016.

Martien, P. T and Harley, R. A.: Adjoint sensitivity analysis for a three-dimensional photochemical model: application to Southern California, Environmental Science & Technology, 40(13), 4200-4210, 2006.

Mesbah, S. M., Hakami, A., and Schott, S.: Optimal Ozone Reduction Policy Design Using Adjoint-Based NOx Marginal Damage Information, Environmental Science & Technology 47(23), 13528-13535, 2013.

Nester, K. and Panitz, H. J.: Sensitivity analysis by the adjoint chemistry transport model DRAISfor an episode in the Berlin Ozone (BERLIOZ) experiment, Atmos. Chem. Phys. 6(8), 2091, 2006.

Pappin, A. J. and Hakami, A.: Source Attribution of Health Benefits from Air Pollution Abatement in Canada and the United States: An Adjoint Sensitivity Analysis, Environmental health perspectives 121(5), 572-579, 2013.

Paulot, F., Jacob, D. J., Pinder, R. W., Bash, J. O., Travis, K. and Henze, D. K.: Ammonia emissions in the United States, European Union, and China derived by high-resolution inversion of ammonium wet deposition data: Interpretation with a new agricultural emissions inventory (MASAGE_NH3), Journal of Geophysical Research: Atmospheres, 4343-4364, 2014.

Sandu, A., Daescu, D. N., Carmichael, G. R., and Chai, T.: Adjoint sensitivity analysis of regional air quality models, Journal of Computational Physics, 204, 222-252, 2005.

Sun, Y. L., Jiang, Q., Wang, Z., Fu, P. Q., Li, J., Yang T., and Yin, Y.: Investigation of the sources and evolution processes of severe haze pollution in Beijing in January 2013, Journal of Geophysical Research: Atmospheres, 119(7), 4380-4398, 2014.

Wang, H., Shi, G. Y., Zhang, X. Y., Gong, S. L., Tan, S. C., Chen, B., Che, H. Z., and Li, T.: Mesoscale modelling study of the interactions between aerosols and PBL meteorology during a haze episode in China Jing-Jin-Ji and its near surrounding region – Part 2: Aerosols' radiative feedback effects, Atmos. Chem. Phys., 15, 3277-3287, 2015a.

Wang, H., Xue, M., Zhang, X. Y., Liu, H. L., Zhou, C. H., Tan, S. C., Che, H. Z., Chen, B., and Li, T.: Mesoscale modelling study of the interactions between aerosols and PBL meteorology during a haze episode in Jing-Jin-Ji (China) and its nearby surrounding region – Part 1: Aerosol distributions and meteorological features, Atmos. Chem. Phys., 15, 3257-3275, 2015b.

Wang, L. T., Wei, Z., Wei, W., Fu, J. S., Meng, C. C., and Ma, S.: Source apportionment of $PM_{2.5}$ in top polluted cities in Hebei, China using the CMAQ model, Atmos. Environ., 122, 723-736, 2015.

Wu, D., Xu, Y., and Zhang S. Q.: Will joint regional air pollution control be more cost-effective? An empirical study of China's Beijing–Tianjin–Hebei region, Journal of Environmental Management, 149, 27-36, 2015.

Xue, J. and Chen, D.: Scientific Design and Application of Numerical Predicting System GRAPES, Science Press, Beijing, 2008.

Yu, L. D., Wang, G. F., Zhang, R. J., Zhang, L. M., Song, Y., Wu, B. B., Li, X. F., An K., and Chu, J. H.: Characterization and Source Apportionment of $PM_{2.5}$ in an Urban Environment in Beijing, Aerosol and Air Quality Research, 13, 574-583, 2013.

Yumimoto, K. and Uno, I.: Adjoint inverse modeling of CO emissions over Eastern Asia using four-dimensional variational data assimilation, Atmos. Environ., 40(35), 6836-6845, 2006.

Zhai, S. X.: Development of the adjoint of GRAPES-CUCAE aerosol module and model application to air pollution optimal control problems, MSc diss., Chinese Academy of Meteorological Sciences, 2015 (in Chinese).

Zhai, S. X., An, X. Q., Liu, Z., Sun, Z. B., and Hou, Q.: Model assessment of atmospheric pollution control schemes for critical emission regions, Atmos. Environ., 124, Part B, 367-377, 2016.

Zhai, S. X., An, X. Q., Liu, J., Wu, Q. Z., Li, N., and Zhang, X. L.: Effects of emission-sources reduction at different time

Atmos. Chem. Phys. Discuss., doi:10.5194/acp-2016-911, 2016
Manuscript under review for journal Atmos. Chem. Phys.
Published: 25 November 2016

Atmospheric Chemistry and Physics Discussions

points on $PM_{2.5}$ concentration over Beijing Municipality, China Environmental Science., 34(6), 1369-1379, 2014 (in Chinese).

Zhang, H. F., Wang, S. X., Hao, J. M., Wang, X. M., Wang, S. L., Chai, F. H., and Li, M.: Air pollution and control action in Beijing, Journal of Cleaner Production, 112, Part 2: 1519-1527, 2016.

Zhang, Q, Streets, D. G., Carmichael, G. R., He, K. B., Huo, H., Kannari, A., Klimont, Z., Park, I. S., Reddy, S., Fu, J. S., Chen, D., Duan, L., Lei, Y., Wang, L. T., and Yao, Z. L.: Asian emissions in 2006 for the NASA INTEX-B mission, Atmos. Chem. Phys., 9(14), 5131-5153, 2009.

Zhang, L., Liu, L. C., Zhao, Y. H., Gong, S. L., Zhang, X. Y., Henze, D. K., Capps, S. L., Fu, T. M., Zhang, Q., and Wang, Y. X.: Source attribution of particulate matter pollution over North China with the adjoint method, Environmental Research Letters 10(8): 084011, 2015.

Zheng, M., Salmon, L. G., Schauer, J. J., Zeng, L., Kiang, C., Zhang, Y., and Cass, G. R.: Seasonal trends in $PM_{2.5}$ source contributions in Beijing, China. Atmos. Environ, 39(22), 3967-3976, 2005.

Zhou C. H., Gong S. L., Zhang X. Y., Liu H. L., Xue M., Cao G. L., An X. Q., Che H. Z., Zhang Y. M., and Niu T.: Towards the improvements of simulating the chemical and optical properties of Chinese aerosols using an online coupled model – CUACE/Aero, Tellus B, 64(0), 2012.

Zíková, N., Wang, Y., Yang, F., Li, X., Tian, M., and Hopke P. K.: On the source contribution to Beijing $PM_{2.5}$ concentrations, Atmos. Environ., 134, 84-95, 2016.

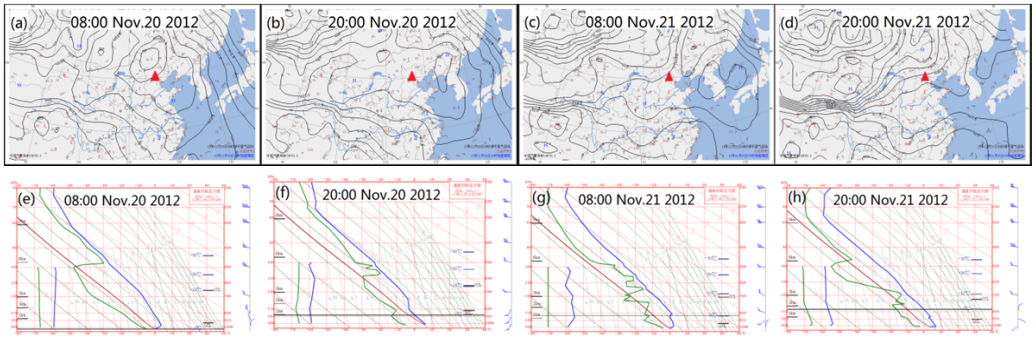

Figure 1. Sea-level pressure field (a-d, Beijing is marked with a red triangle), the Stratification and the dew point-pressure curves at Nanjiao Station (e-h) from 08:00 BT Nov. 20th 2012 to 20:00 BT Nov. 21st 2012.

Atmos. Chem. Phys. Discuss., doi:10.5194/acp-2016-911, 2016
Manuscript under review for journal Atmos. Chem. Phys.
Published: 25 November 2016

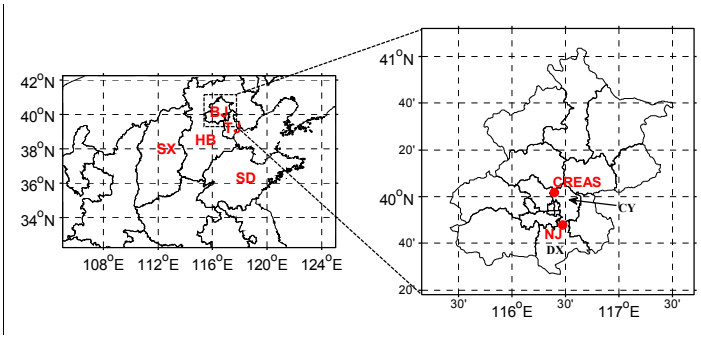

Figure 2. Left: Model domain settings and location of Beijing municipality (BJ), Tianjin municipality (TJ), Heibei province (HB), Shandong province (SD) and Shanxi province (SX) ; right: Locations of the Chinese Research Academy of Environmental Sciences (CREAS) station, the Nanjiao (NJ) station, Daxing district (DX) and Chaoyang (CY) district.

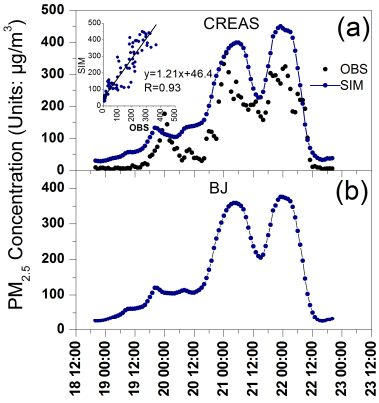

Figure 3. (a): Comparisons of the observed (black solid dots) and simulated (blue dot-line) hourly $PM_{2.5}$ concentrations at CREAS station and their scatter plots (at the top-left corner); (b): Hourly variations of average $PM_{2.5}$ concentration over Beijing municipality.

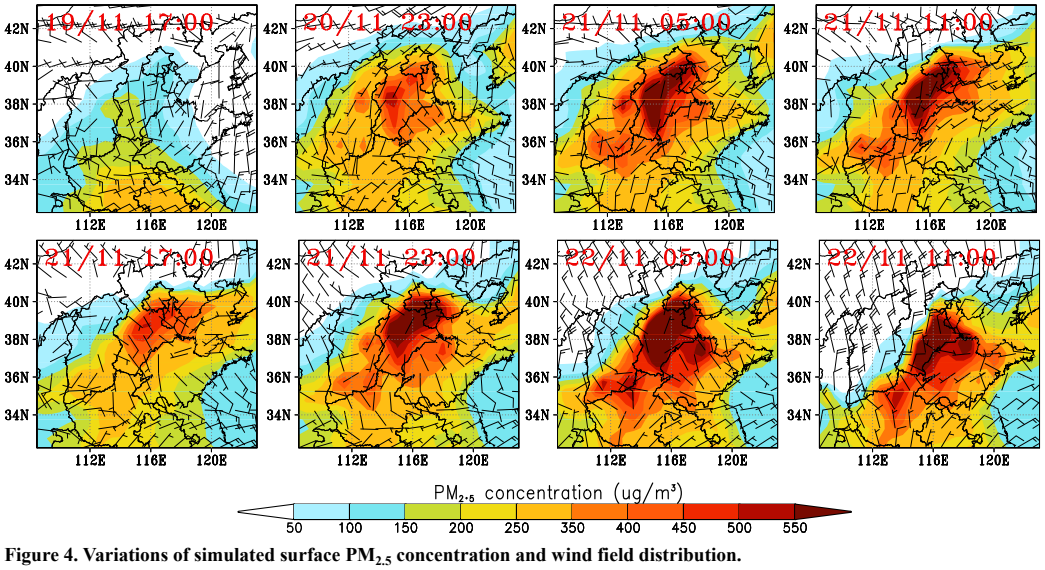

Figure 4. Variations of simulated surface $PM_{2.5}$ concentration and wind field distribution.

Atmos. Chem. Phys. Discuss., doi:10.5194/acp-2016-911, 2016
Manuscript under review for journal Atmos. Chem. Phys.
Published: 25 November 2016

Atmospheric Chemistry and Physics Discussions

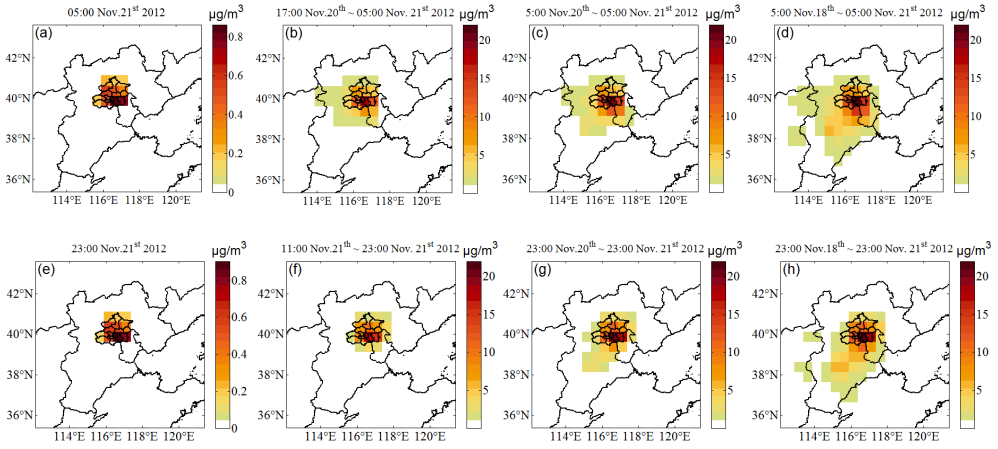

Figure 5. Time-integrated sensitivity coefficients of surface Beijing $PM_{2.5}$ concentration peaks to primary emission sources. (a)-(d): 1-h, 12-h, 24-h and 72-h integrated sensitivity coefficients for the 5:00 BT Nov. 21st $PM_{2.5}$ concentration peak; (e)-(h): 1-h, 12-h, 24-h and 72-h integrated sensitivity coefficients for the 23:00 BT Nov. 21st $PM_{2.5}$ concentration peak.

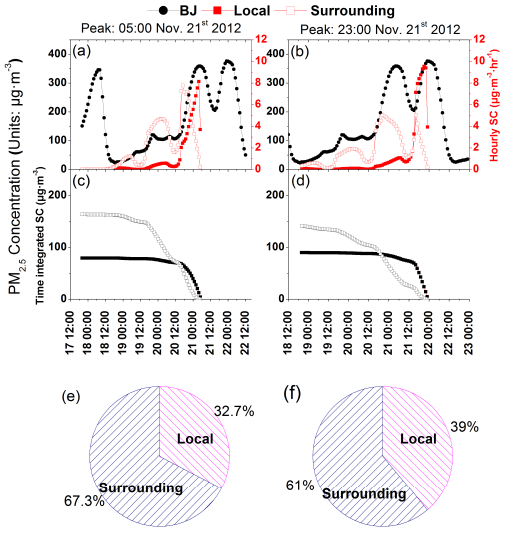

Figure 6. Hourly variations of surface Beijing $PM_{2.5}$ concentration and sensitivity coefficients of surface Beijing $PM_{2.5}$ concentration peaks to local and surrounding primary emission sources. The left and right panels correspond to $PM_{2.5}$ concentration peaks on 05:00 BT and on 23:00 BT Nov. 21st 2012 respectively. (a)-(b) illustrate hourly variations of Beijing $PM_{2.5}$ concentration (black solid dot-line) and hourly instantaneously sensitivity coefficients to local (red solid square) and surrounding (red hollow square) emission sources. (c)-(d) show the time-integrated sensitivity coefficients to local (black solid square) and surrounding (black hollow square) emission sources. (e)-(f) are the contribution ratios of local and surrounding emission sources to $PM_{2.5}$ concentration peaks.

Atmos. Chem. Phys. Discuss., doi:10.5194/acp-2016-911, 2016
Manuscript under review for journal Atmos. Chem. Phys.
Published: 25 November 2016

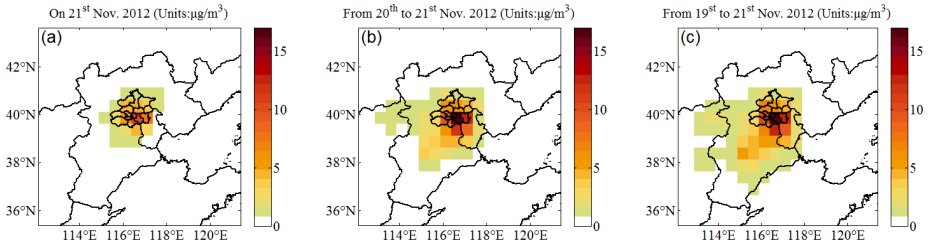

Figure 7. 24-h (a), 48-h (b) and 72-h (c) integrated sensitivity coefficients of surface Beijing $PM_{2.5}$ concentration on Nov. 21st 2012 to primary emission sources.

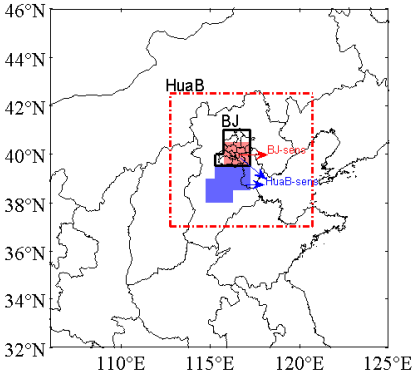

Regions	Number of grid cells	Sensitive area ratios
HuaB-sens	18	10.2%
HuaB	176	
BJ-sens	6	60.0%
BJ	10	

Figure 8. Domain definition of Huabei (HuaB, in red dot-dashed frame), Beijing (BJ, in black solid frame), sensitive Beijing (BJ-sens, red shaded) and sensitive Huabei (HuaB-sens, red shaded and blue shaded) regions.

Notes: HuaB-sens area ratio = 'HuaB-sens floor space'/'HuaB floor space'×100%;

BJ-sens area ratio = 'BJ-sens floor space'/'BJ floor space'×100%.

Atmos. Chem. Phys. Discuss., doi:10.5194/acp-2016-911, 2016
Manuscript under review for journal Atmos. Chem. Phys.
Published: 25 November 2016

Atmospheric Chemistry and Physics Discussions

Table 1 Primary emission sources contribution to the average $PM_{2.5}$ concentration over Beijing on Nov 21st.

Factors	Time period	BJ	BJ-sens	HuaB	HuaB-sens
SC/PC	d0	14.5%	12.5%	25.6%	18.4%
	d1	20.7%	18.3%	57.5%	37.3%
	d2	21.3%	18.8%	67.1%	40.9%

Notes: d0 refers to emissions contribution on 21st Nov.; d1 refers to emissions contribution from 20th to 21st Nov.; d2 refers to emissions contribution from 19th to Nov. 21st.

SC/PC='time cumulative Sensitivity Coefficient'/'Peak Concentration';

5

Atmos. Chem. Phys. Discuss., doi:10.5194/acp-2016-911, 2016
Manuscript under review for journal Atmos. Chem. Phys.
Published: 25 November 2016

Atmospheric Chemistry and Physics Discussions

Table 2 Contrast of sensitive and full region emission sources contribution

GRAPES-CUACE aerosol adjoint model results				Models-3/CMAQ results (Zhai et al., 2016)	
Time period	Factors	BJ-sens	HuaB-sens	BJ-sens	HuaB-sens
d0	S/F(effect)	86.6%	71.9%		
	S/F(efficiency)	1.4	7.0		
d1	S/F(effect)	88.2%	64.9%	99.2%	93.7%
	S/F(efficiency)	1.5	6.3	1.8	5.3
d2	S/F(effect)	88.2%	61.0%	100.8%	87.2%
	S/F(efficiency)	1.5	6.0	1.9	5.0

Notes: S/F(effect) = 'Sensitivity Coefficient over sensitive source region'/'Sensitivity Coefficient over corresponding full source region';
Contribution Efficiency= 'Sensitivity Coefficient'/'Number of region's simulation grid cells';
S/F(efficiency)= 'Contribution Efficiency of sensitive region'/'Contribution Efficiency of corresponding full source region'.

5